scientific reports

Check for updates

OPEN

Assessment of choroidal vessels in healthy eyes using 3-dimensional vascular maps and a semi-automated deep learning approach

Nicola Valsecchi[1,2,3], Elham Sadeghi[1], Elli Davis[1], Mohammed Nasar Ibrahim[1], Nasiq Hasan[1], Sandeep Chandra Bollepalli[1], Sumit Randhir Singh[4], Luigi Fontana[2,3], Jose Alain Sahel[1], Kiran Kumar Vupparaboina[1] & Jay Chhablani[1]✉

To assess the choroidal vessels in healthy eyes using a novel three-dimensional (3D) deep learning approach. In this cross-sectional retrospective study, swept-source OCT 6 × 6 mm scans on Plex Elite 9000 device were obtained. Automated segmentation of the choroidal layer was achieved using a deep-learning ResUNet model along with a volumetric smoothing approach. Phansalkar thresholding was employed to binarize the choroidal vasculature. The choroidal vessels were visualized in 3D maps, and divided into five sectors: nasal, temporal, superior, inferior, and central. Choroidal thickness (CT) and choroidal vascularity index (CVI) of the whole volumes were calculated using the automated software. The three vessels for each sector were measured, to obtain the mean choroidal vessel diameter (MChVD). The inter-vessel distance (IVD) was defined as the distance between the vessel and the nearest non-collateral vessel. The choroidal biomarkers obtained were compared between different age groups (18 to 34 years old, 35 to 59 years old, and ≥ 60) and sex. Linear mixed models and univariate analysis were used for statistical analysis. A total of 80 eyes of 53 patients were included in the analysis. The mean age of the patients was 44.7 ± 18.5 years, and 54.7% were females. Overall, 44 eyes of 29 females and 36 eyes of 24 males were included in the study. We observed that 33% of the eyes presented at least one choroidal vessel larger than 200 µm crossing the central 3000 µm of the macula. Also, we observed a significant decrease in mean CVI with advancing age ($p < 0.05$), whereas no significant changes in mean MChVD and IVD were observed ($p > 0.05$). Furthermore, CVI was increased in females compared to males in each sector, with a significant difference in the temporal sector ($p < 0.05$). MChVD and IVD did not show any changes with increasing age, whereas CVI decreased with increasing age. Also, CVI was increased in healthy females compared to males. The 3D assessment of choroidal vessels using a deep-learning approach represents an innovative, non-invasive technique for investigating choroidal vasculature, with potential applications in research and clinical practice.

Keywords Choroidal vessels, OCTA, 3D, Choroidal vascularity index, Healthy eyes

The choroid is the most vascular structure of the eye and one of the most complex networks in the human body[1]. It lays between the retinal pigment epithelium (RPE) and the sclera, and it supplies the photoreceptor cells in the outer retina by delivering oxygen and removing metabolic waste products[2]. The choroid has been extensively studied for over a decade, resulting in the identification of several clinically significant biomarkers[3,4]. The choroidal vascularity index (CVI) has emerged as a key tool for assessing choroidal vessels, utilizing both en-face and cross-sectional imaging modalities to evaluate choroidal structure and function[5–7]. Despite its widespread use, these imaging techniques face limitations in providing a truly precise analysis of the choroidal vasculature. This challenge arises from the inherently non-uniform and irregular distribution of choroidal vessels, which contrasts with the more orderly and predictable arrangement of retinal vessels[2]. The complexity and variability in the choroidal vessel architecture introduce difficulties in accurately quantifying and interpreting choroidal

[1]Department of Ophthalmology, School of Medicine, University of Pittsburgh, Pittsburgh, PA, USA. [2]Ophthalmology Unit, Dipartimento di Scienze Mediche e Chirurgiche, Alma Mater Studiorum University of Bologna, Bologna, Italy. [3]IRCCS Azienda Ospedaliero-Universitaria di Bologna, Bologna, Italy. [4]Sri Sai Lions Netralaya and Sri Sai Eye Hospital, Patna, Bihar 800020, India. ✉email: jay.chhablani@gmail.com

changes. Thus, three-dimensional (3D) imaging is needed to accurately measure the real diameter and structure of choroidal vessels, providing a more comprehensive understanding of their morphology.

In recent years, the introduction of swept source OCT (SS-OCT) systems has significantly increased image acquisition speed and resolution. Also, the longer wavelength of SS-OCT enables better penetration into the choroid, thereby enhancing scan quality for in vivo choroidal assessment[8,9]. Furthermore, the introduction of deep learning methods for choroid vessel segmentation have been developed, showing promising results for quantifying choroidal biomarkers[10–14]. Several studies have attempted to measure the diameter of choroidal vessels in two-dimensional scans[15–17]. However, none have succeeded in developing a method to quantify choroidal vessels within 3D maps and to understand the spatial and anatomical relationships between the large choroidal vessels.

To address these limitations, we present a semi-automated deep-learning technique capable of generating 3D reconstructions of the Haller layer, along with a methodology for measuring choroidal vessel diameter, inter-vessel distance, CVI, and choroidal thickness (CT) in different sectors of the choroid. Therefore, our main objective is to assess these choroidal biomarkers in a cohort of healthy patients, utilizing this innovative 3D deep learning approach.

Materials and methods

Study population

In this cross-sectional retrospective study, we included eyes of healthy individuals who were routinely followed in our hospital for regular ophthalmic evaluations. The study was conducted at the Medical Retina and Vitreoretinal Surgery, University of Pittsburgh School of Medicine, from January 2022 to February 2024. The study adhered to the tenets of the Declaration of Helsinki. Informed consent was obtained from all the patients included in the study. Ethical clearance was obtained by the institutional review board of the University of Pittsburgh. We included eyes of healthy patients more than 18 years old, availability of detailed information regarding the clinical history of the patients, and high-definition-OCT images. We excluded patients with a history of any intraocular pathology, surgery (except uncomplicated cataract surgery), inflammation, glaucoma, axial length < 22 mm and > 26 mm, and trauma. Also, we excluded patients with systemic diseases with potential ophthalmological involvement, such as diabetes, uncontrolled systemic hypertension, impaired renal function, and thyroid disorders.

Clinical assessment

Each individual included in the study received a comprehensive evaluation of ophthalmological, systemic, and familial history, visual acuity and refraction assessment, measurement of intraocular pressure, external eye examination, slit lamp examination, and fundus examination. These examinations were meticulously performed to systematically exclude any potential abnormalities involving the cornea, lens, anterior chamber, vitreous, retina, optic nerve, choroid, and sclera. Axial length was measured using the IOLMaster 700 (Carl Zeiss Meditec, Jena, Germany).

OCT imaging acquisition

Following pupillary dilation, SS-OCT images of 6×6 mm area centered on the fovea were captured on the Plex Elite 9000 device (Carl Zeiss Meditec, Dublin, CA). The in-built scoring system in the SS-OCT software graded the quality of the scans. Scans with scores ≥ 6 (highlighted in green) out of 10 were included in the analysis. Each OCT volume comprised of 1024 B-scans and the resolution of each scan was 1024×1536. Only eyes with normal OCT scans assessed by two graders (NV, ES) and high-quality acquisitions were accepted for this study. Overall, a total of 107 eyes from 64 patients were reviewed in our study. Of these, 23 eyes were excluded due to poor image quality, and 2 eyes were excluded due to pathological changes identified in the OCT scans.

Automated choroidal vessel segmentation

The suggested approach includes a variety of automated and manual subtasks designed to measure the cross-sectional diameter (CSD) of 3D choroidal vessels. A crucial step in this process is accurately modeling the complex choroidal vasculature from volumetric SS-OCT scans. To accomplish this, we started by algorithmically defining the boundaries of the choroid layer from the structural SS-OCT volume, then proceeded to segment the choroidal vessels in each B-scan. The vessels detected in the B-scans were then collated, and morphological operations were applied to produce a smooth 3D choroidal vasculature model. The choroid layer delineation process involves detecting the (i) choroid inner boundary (CIB) and (ii) choroid outer boundary (COB). The CIB was delineated along the junction between the choroid and the retinal pigment epithelium, while the COB was traced along the junction between the choroid and the sclera. Considering the effectiveness of deep learning (DL) methods in segmenting the choroidal layer, both in terms of accuracy and execution time, we adopted a DL framework. Specifically, we used our previously developed approaches, which involve a residual encoder-decoder DL model, followed by volumetric smoothing[10,14]. To train the DL-based algorithm, we used our previously reported volumetric segmentation method[14]. To circumvent spurious choroid boundary segmentations, we added the manual boundary correction step. In this study, the algorithm demonstrated an accuracy of 92.3% in delineating the choroidal boundaries in healthy eyes, with manual correction required for the remaining cases. See Fig. 1. The steps described above and shown in Fig. 1 are represented in Fig. 2 with examples of OCT images.

We segmented the choroidal vessels from SS-OCT volume based on algorithmically delineated choroidal layer. Segmenting choroidal vasculature is challenging because of its complex structure and intensity profile. Choroidal vessels are densely interwoven, and the OCT acquisition process can introduce artifacts like speckle noise, retinal shadows, contrast variation, and misaligned B-scans. To address these issues, we employed the Phansalkar thresholding method, previously reported by our group, for the task of choroidal vessel segmentation.

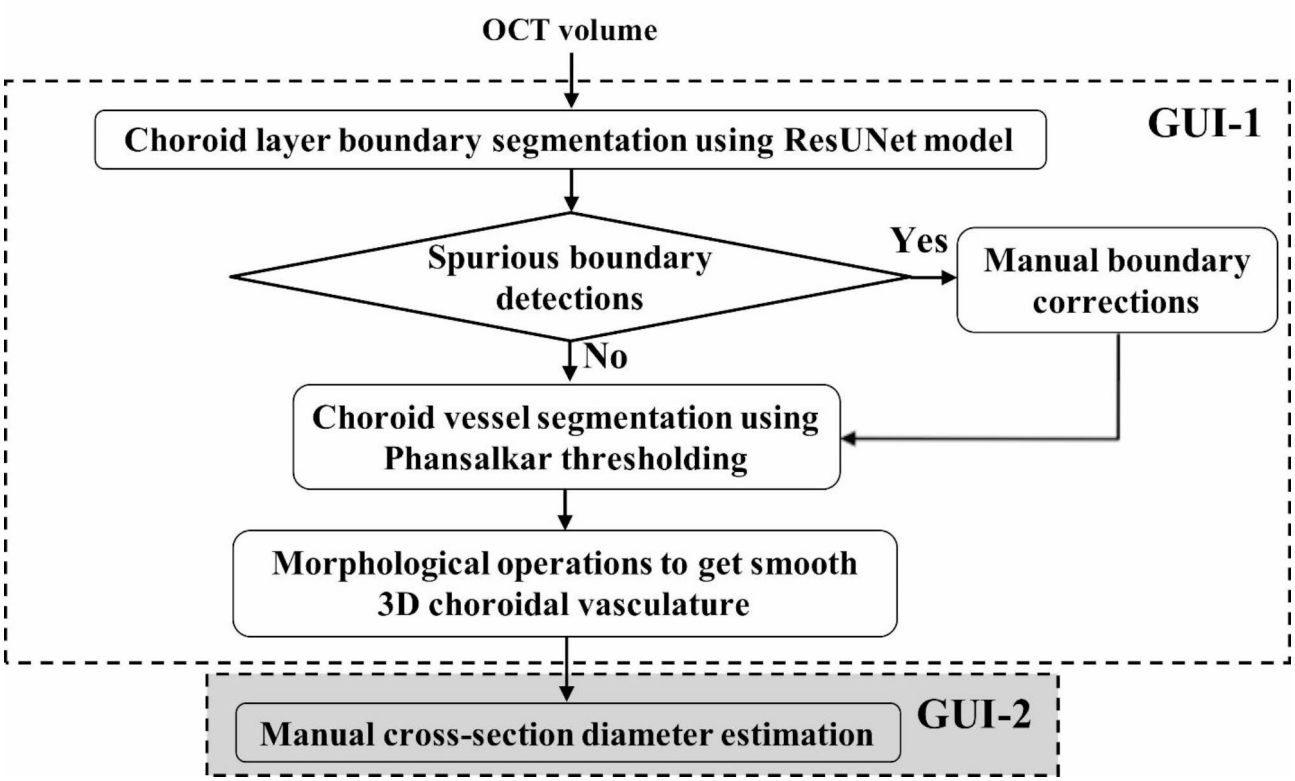

Fig. 1. The figure shows the workflow of the choroid layer boundary segmentation. *GUI* graphical user interface.

This method estimates the local threshold in each overlapping window of tile size 16×16 pixels in each B-scan to differentiate between luminal and stromal regions[18]. Subsequently, post-processing morphological operations were employed to eliminate extraneous components and produce a smooth 3D representation of the choroidal vasculature. To assist graders with the automated and manual tasks in the proposed methodology, we developed two graphical user interfaces (GUI-1 and GUI-2). GUI-1 was designed to accurately derive 3D choroidal vasculature from OCT volumes and accepted raw SS-OCT input in IMG or JPG format. It includes functionalities for performing automated subtasks, such as choroid boundary segmentation using either a model or a multi-ResUNet model. The automated segmentation results can be reviewed and manually corrected if necessary. Then, ImageJ 1.51 s (National Institutes of Health, Bethesda, MD) was used to mask the choroidal vasculature in the location of the optic disc. Finally, the choroid vessel segmentation is completed, and the 3D choroid vasculatures are saved for manually measuring the cross-sectional diameter in GUI-2. All 3D choroidal vasculature data prepared using GUI-1 are subsequently integrated into GUI-2 for CSD measurement.

In GUI-2, all OCT volumes are listed for the grader to select from. Once a volume is selected, the corresponding en-face image is displayed, and the user is prompted to mark the foveal center, which is the center of the foveal avascular zone area in correlation with cross-sectional B scan. This action positions a 6×6 grid on the 3D choroidal vasculature, centered at the fovea. The central sector is a circle with a 2 mm diameter. When the grader clicks the "perform vessel measurement" button, the vasculature with the grid is shown, highlighting different sectors (nasal, temporal, superior, inferior, and central).

The grader can select any point within a sector, opening a window that shows the small vasculature around that point. This enables the grader to measure the cross-sectional diameter of a vessel by clicking on its opposite edges. The measured values are then recorded in an Excel sheet for further analysis. After segmenting choroidal vessels and applying binarization with Phansalkar thresholding, two eyes were excluded from the analysis due to inadequate visualization of the choroidal vessels in the 3D maps.

Assessment of choroidal vessel diameter and inter-vessel distance

The analysis involved selecting the three largest vessels in each sector of the 3D map. Before choosing the vessels, the images were rotated to provide a comprehensive three-dimensional view.

The vessels were positioned to enable a precise and thorough assessment of their diameters. To determine the cross-sectional diameter, measurements were made from the outermost visible edges of each vessel, with three measurements taken for each. These measurements were randomly selected along the straight sections of the vessels, deliberately avoiding regions near bifurcations or the origins of collateral vessels to prevent inaccuracies in diameter estimation.

In cases of uncertainty, four or more vessels were measured, and the measurements from the three largest vessels were selected for analysis to ensure an objective assessment of the largest vessels in each sector. The mean

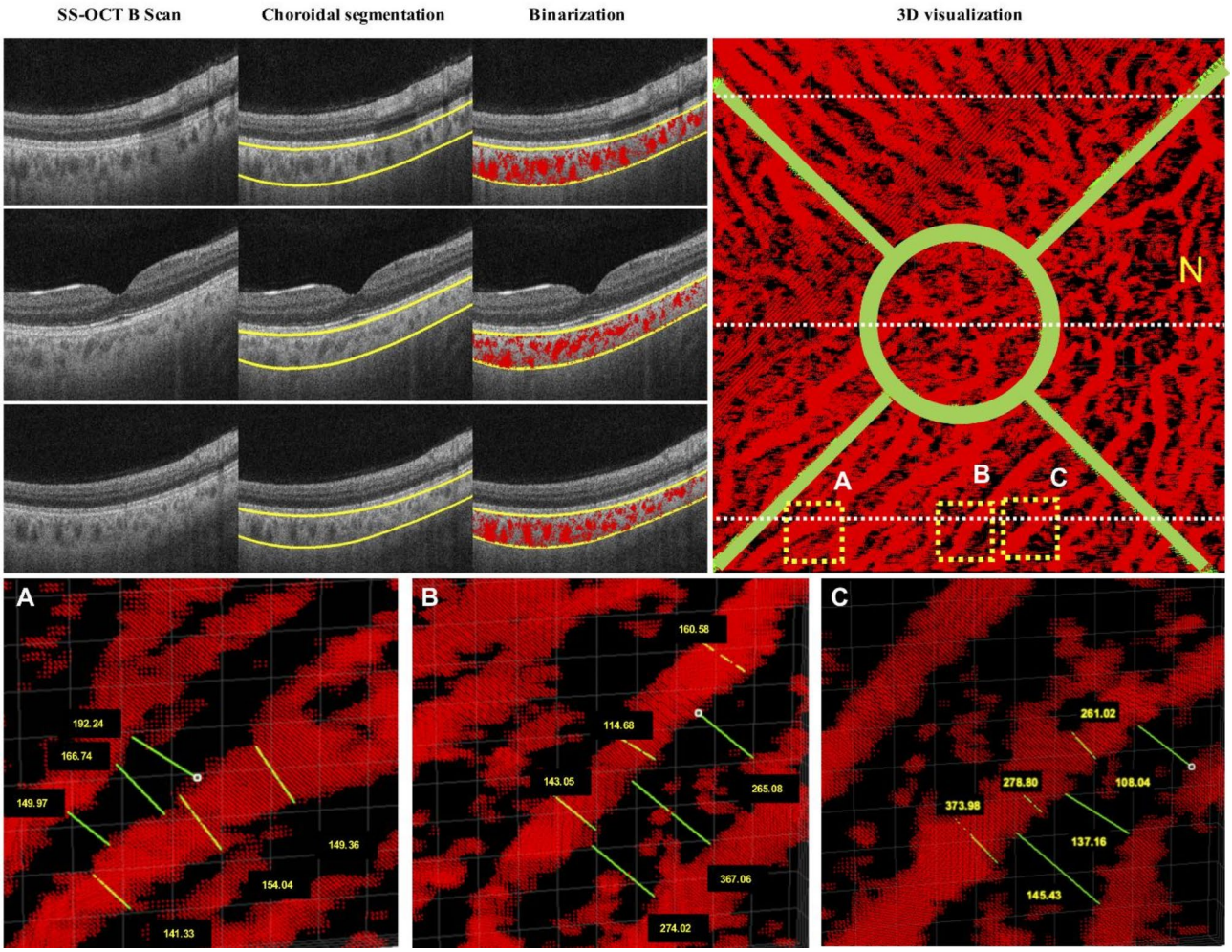

Fig. 2. Choroidal vessel segmentation and assessment of the mean choroidal vessel diameter (MChVD) and inter-vessel distance (IVD) in a healthy eye. The images on the top left show the swept-source optical coherence tomography scans of the right eye of a healthy patient with automated segmentation of the choroid inner and outer boundary and binarization of the choroidal vessels through the Phansalkar thresholding method. The image on the top right shows the three-dimensional 6 × 6 mm map. The horizontal white dashed-lines in the 3D map correspond to the OCT-B scan for that level. One point is selected in the inferior sector (yellow circles) The images at the bottom show the magnification of the point chosen, and the measurements taken. Three points were chosen to correspond to the three largest vessels in the inferior sector. At each point, three independent measurements were taken to assess the diameter of the largest vessel. The IVD was obtained considering the distance between the largest vessel chosen and the nearest independent non-collateral vessel. The mean of the 9 diameters was calculated, representing the MChVD of the inferior sector for this eye. The mean of the 9 IVD was calculated, representing the mean of the IVD in the inferior sector of this specific eye. Values are reported in μm.

choroidal vessel diameter (MChVD) for each sector was calculated by averaging the 9 measurements (3 per vessel). The inter-vessel distance was defined as the distance between one of the largest vessels and the nearest independent, non-collateral vessel in each sector. To determine the mean inter-vessel distance, three different measurements were randomly taken for each of the three largest vessels per sector, resulting in a total of 9 measurements (3 per vessel). In summary, 18 measurements were collected per sector (9 for MChVD and 9 for inter-vessel distance), amounting to a total of 90 measurements per eye, as previously described[19]. Additionally, the mean value of the five sectors was calculated to provide a global assessment of each choroidal biomarker for each eye. See Fig. 2. A representative video of GUI-2 is shown in **Supplementary file 1**. The selection of the vessels and the measurements were performed by two graders blinded to patients' characteristics. (N.V., E.D.). The measurements from the first grader (N.V.) were used for the analysis, whereas the measurements from the second grader (E.D.) were used to assess the inter-grader reliability. The choroidal thickness (CT) and the CVI of the whole volume were calculated through the automated software. Furthermore, each scan was assessed in the central 3000 μm of the macula to define the number of eyes presenting at least one choroidal vessel larger than 200 μm, in order to report their number and describe their pathway.

Statistical analysis

Normality was tested with the Shapiro–Wilk test and parametric tests were used for the analysis. The inter-rater reliability for image binarization was assessed using the absolute agreement model of the intra-class correlation coefficient (ICC). The chi-square test was used for categorical variables. Linear mixed models were used in the statistical analysis to account for correlation between the two eyes of each patient. The choroidal biomarkers were assessed among the different patients' genders. Also, the choroidal biomarkers were assessed among different age groups (18 to 34 years old, 35 to 59 years old, and ≥ 60), and the Bonferroni correction was applied for multiple comparisons. Furthermore, univariate analysis was performed to assess the relationship between the choroidal biomarkers and age and AL. *P* values < 0.05 were considered statistically significant. Statistical analysis was performed using IBM Statistical Package for Social Sciences version 26.

Results

Demographic data and choroidal biomarkers

A total of 80 eyes of 53 patients were included in the analysis. The mean age of the patients was 44.7 ± 18.5 years, and 54.7% were females. Overall, 44 eyes of 29 females and 36 eyes of 24 males were included in the study. Demographic data are shown in Table 1.

Overall, the measurements by both readers showed a good level of agreement (ICC = 0.864, CI 0.801–0.912). The CT was thicker in the central sector (309.5 ± 83.9), followed by the inferior (299.3 ± 73.5), superior (287.1 ± 77.0), temporal (281.8 ± 72.9) and nasal (244.6 ± 63.5) sectors. The sector with the highest CVI was the superior, followed by the inferior, central, nasal, and temporal. The sector with the highest MChVD was the inferior, followed by the superior, nasal, temporal, and central. On the other hand, the highest IVD was found in the superior sector, followed by the temporal, inferior, central, and nasal. See Table 2. We did not find any correlations between MChVD and CT in the nasal (r=-0.019, $p = 0.869$), inferior ($r = 0.158$, $p = 0.168$), and in the central sector ($r = 0.120$, $p = 0.288$). On the other hand, we observed a positive correlation in the temporal ($r = 0.241$, $p = 0.031$) and in the superior sectors ($r = 0.239$, $p = 0.034$).

We observed that 33% of the eyes presented at least one choroidal vessel larger than 200 µm crossing the central 3000 µm of the macula. A single vessel was noted in 18% of the cases, whereas multiple vessels were observed in 15% of the cases (2 vessels in 12% of the cases, 3 vessels in 2% of the cases). Their pathway was oblique (from the inferotemporal to the superonasal sectors) in 62% of the cases, vertical in 29% of the cases, and horizontal in 7% of the cases. Among the eyes with multiple vessels crossing the fovea, they presented a parallel course in 84% of the cases and a divergent course in 16%. See Figs. 3 and 4. The representation of the 3D map of the eye in Fig. 4 is shown in **Supplementary video 2.**

Choroidal biomarkers in different age groups

No significant differences were observed between the three age groups (18 to 34 years old, 35 to 59 years old, and ≥ 60) regarding axial length (23.9 ± 0.9 vs. 23.7 ± 1.0 vs. 24.3 ± 0.9 mm, $p = 0.407$), and sex (females 46.4% vs. 53.3% vs. 68.1%, $p = 0.300$). The mean CT was significantly higher in the 18–34 age group compared to other age groups ($p = 0.009$). After Bonferroni correction, the differences between age group 18–34 and 35–59 ($p = 0.018$), age group 18–34 and > 60 ($p = 0.018$), and 35–59 and > 60 ($p = 0.020$) remained statistically significant. Also, we noted that the mean CVI was significantly increased in the age group 18–34 compared to the other groups ($p = 0.002$). After Bonferroni correction, the differences between age group 18–34 and 35–59 ($p = 0.005$), age group 18–34 and > 60 ($p = 0.015$), and 35–59 and > 60 ($p = 0.015$) remained statistically significant. We did not observe any significant differences among the different age groups for the mean MChVD. On the other hand, we observed a significantly increased IVD for the age group 35–59 compared to the other groups in the inferior and central sectors ($p < 0.05$). After Bonferroni correction, the IVD in the inferior sector between age group 18–34 and 35–59 ($p = 0.063$), age group 18–34 and > 60 ($p = 0.072$), and 35–59 and > 60 ($p = 0.072$) was not statistically significant. On the other hand, the IVD in the central sector was statistically significant between the age group 35–59 and > 60 ($p = 0.034$), whereas it was not statistically significant for the age group 18–34 and 35–59 ($p = 0.774$), and age group 18–34 and > 60 (0.371). See Table 3.

Choroidal biomarkers according to gender

No significant differences between males and females were observed regarding axial length (24.2 ± 1.0 vs. 23.7 ± 0.9 mm, $p = 0.136$), and age (42.1 ± 18.3 vs. 43.9 ± 18.4 years, $p = 0.106$). The CT was increased in males

Patients	***N* = 53**
Age years, mean ± SD	44.7 ± 18.5
Sex females, n (%)	29 (54.7%)
Eyes	***N* = 80**
Right eye, n (%)	38 (47.5%)
BCVA LogMar, mean ± SD	0.01 ± 0.03
Pseudophakia, n (%)	8 (10%)
Axial length (mm), mean ± SD	23.9 ± 0.9

Table 1. Demographic data are reported. *SD* standard deviation; *BCVA* best corrected visual acuity.

	N = 80
Choroidal thickness (μm), mean ± SD	
Mean	282.3 ± 66.7
Nasal	244.6 ± 63.5
Temporal	281.8 ± 72.9
Inferior	299.3 ± 73.5
Superior	287.1 ± 77.0
Central	309.5 ± 83.9
Choroidal vascularity index (μm), mean ± SD	
Mean	40.3 ± 2.8
Nasal	39.9 ± 4.0
Temporal	39.5 ± 2.9
Inferior	41.0 ± 2.3
Superior	42.1 ± 2.7
Central	40.1 ± 2.7
Mean choroidal vessel diameter (MChVD) (μm), mean ± SD	
Mean	200.4 ± 25.3
Nasal	199.4 ± 44.4
Temporal	195.1 ± 39.6
Inferior	212.2 ± 38.6
Superior	205.8 ± 37.7
Central	193.8 ± 40.3
Inter-vessel distance (IVD) (μm), mean ± SD	
Mean	185.4 ± 35.1
Nasal	177.3 ± 44.9
Temporal	188.5 ± 53.4
Inferior	186.4 ± 47.7
Superior	189.1 ± 49.1
Central	185.5 ± 46.0

Table 2. Three-dimensional assessment of the choroidal vascular biomarkers in healthy eyes. *SD* standard deviation; *MChVD* mean choroidal vessel diameter; *IVD* inter-vessel distance.

compared to females in each sector, even though the differences were not statistically significant ($p > 0.05$). On the other hand, the CVI was increased in females compared to males in each sector, with a significant difference in the temporal sector ($p < 0.05$). Also, the MChVD was higher in females compared to males in each sector, with a significant difference in the nasal sector ($p = 0.019$). Moreover, the IVD was higher in females in each sector, with a significant difference in the superior sector ($p = 0.034$). See Table 4.

Association of choroidal biomarkers with age and axial length

We noted a significant decline in CT with advancing age in the temporal, inferior, superior, and central sectors, whereas no significant correlation was found in the nasal sector. Also, we observed a significant decrease in the CVI with advancing age in the nasal, temporal, superior, and central sectors, whereas no significant correlations were observed for the inferior sector. On the other hand, we did not observe any significant changes according to age for MChVD and IVD. See Table 5.

Furthermore, we observed a reduction of CT with increasing AL in the inferior, superior, and central sectors, whereas no differences were observed in the nasal and temporal sectors. On the other hand, the CVI did not change with increasing axial length. Also, we observed a significant decline in MChVD in the nasal sector ($p = 0.034$) and a significant decline in the IVD in the temporal sector ($p = 0.030$) with increasing AL. No statistically significant differences were observed for the other parameters. See Table 6.

Discussion

In the present study, we found that CVI decreased with increasing age. Also, we observed that MChVD and the IVD were higher in females compared to males in each sector, with a significant difference in the nasal ($p = 0.019$) and the superior sector ($p = 0.034$), respectively. Also, CVI was increased in females compared to males in each sector, with a significant difference in the temporal sector ($p = 0.031$). Furthermore, we noted that

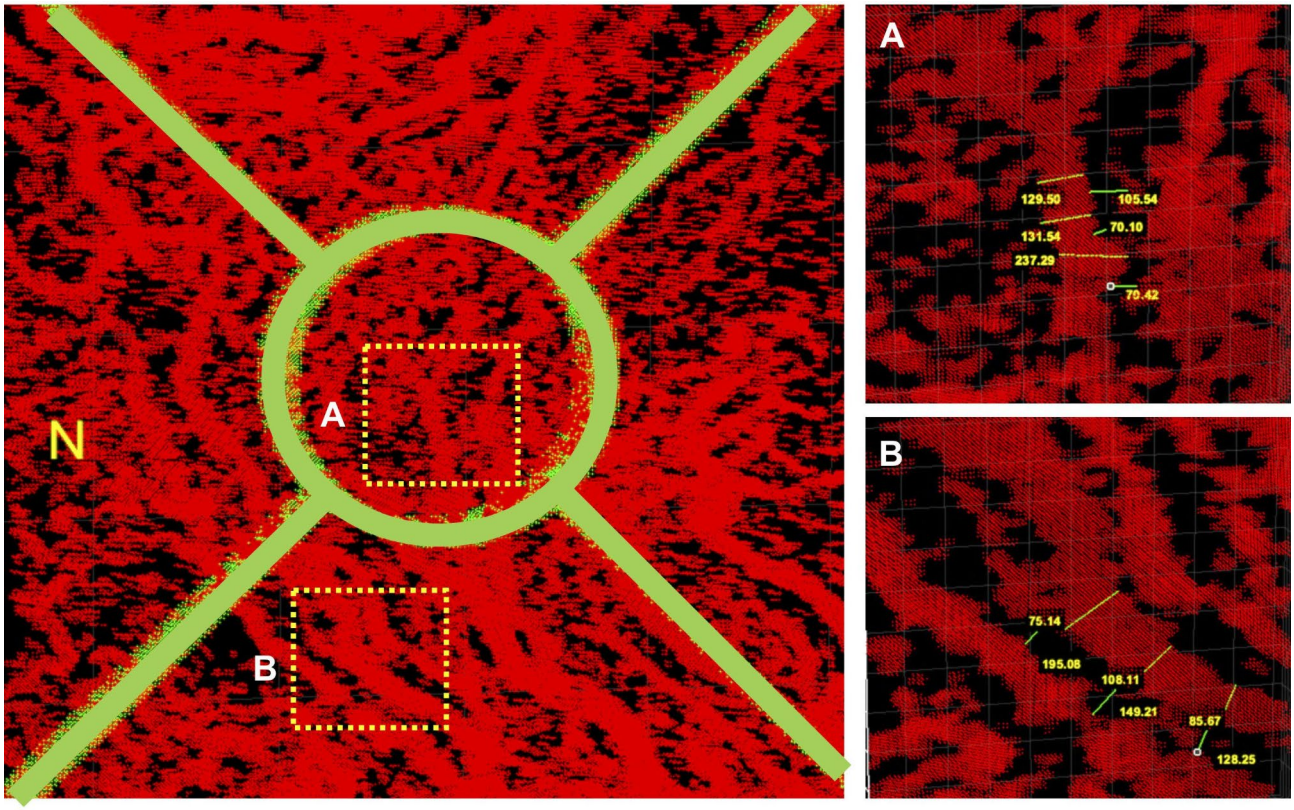

Fig. 3. Choroidal vessels in a healthy 45-year-old female. The image on the left shows the 3D en-face image. The magnified images are shown on the right. (A) In the central sector, the mean of the three measurements for the largest choroidal vessel was 166 µm. The vessel presented a vertical pathway. (B) One of three largest vessels in the inferior sector is shown. The choroidal vessel diameter and the inter-vessel distance were calculated.

33% of the eyes presented at least one choroidal vessel larger than 200 µm crossing the central 3000 µm of the macula.

The peculiarity of the present study is that we implemented an automated DL algorithm to visualize and measure the choroidal vessels in 3D using SS-OCT acquisition. This innovative approach allows for quantifying choroidal vessel diameters non-invasively, and it provides a 3D assessment of the CVI and CT, potentially improving the accuracy of these biomarkers. Previous studies have predominantly focused on assessing choroidal biomarkers using OCT B-scans or volume reconstructions of the choroidal vasculature. Yang et al. assessed the 3D CVI in treatment-naïve acute central serous chorioretinopathy, fellow eyes, and controls[20]. Similarly, Zeng et al. assessed the 3D CVI in eyes affected by central serous chorioretinopathy in ultra-field SS-OCTA scans[17]. However, these approaches did not provide a comprehensive 3D evaluation of the choroidal vasculature to explore the spatial and anatomical relationships among large choroidal vessels. Moreover, they did not develop a method to quantify individual choroidal vessels. The application of 3D maps provided essential spatial context, enabling a more robust identification and analysis of the choroidal vessels. While our primary analysis involved measuring the cross-sectional diameters of vessels, the 3D maps guided the selection of optimal cross-sections, ensuring that the measurements were accurate and representative of the vessel's true anatomy. This integration of 2D metrics with 3D spatial information offers a more precise and comprehensive evaluation of the choroidal vasculature compared to traditional 2D approaches.

The MChVD is novel biomarker that estimate the diameter of the largest choroidal vessels within a specific sector, whereas IVD is a parameter that assesses the three-dimensional relationships among choroidal vessels in Haller's layer. Our findings support the hypothesis that the diameter of the largest choroidal vessels and the spatial relationships between vessels do not change with aging in healthy eyes. Conversely, we noted a decrease in both the diameters and the spacing between choroidal vessels with increasing axial length, indicating that the anatomy and the spatial relationships between choroidal vessels may differ based on the dimensions of the eye.

The relationship between CVI, age, and axial length is controversial. Agrawal et al. reported that CVI was affected by sub-foveal CT, but it was not affected by most of the physiological variables, including AL, age, and intra-ocular pressure[6]. On the other hand, Ruiz Medrano et al. reported that CVI was significantly higher in subjects under 18 years of age than in older subjects[21]. Similarly, Xuan et al. observed that CVI was affected by age, with a decreased by −0.13% with each 1-year increase in age, and it was affected by AL, with a decrease by −2.10% with each 1 mm increase in AL in single scan OCT[22]. Previous studies showed that during aging, a variety of choroidal cell types undergo specific changes. For example, choroidal endothelial cells increase in

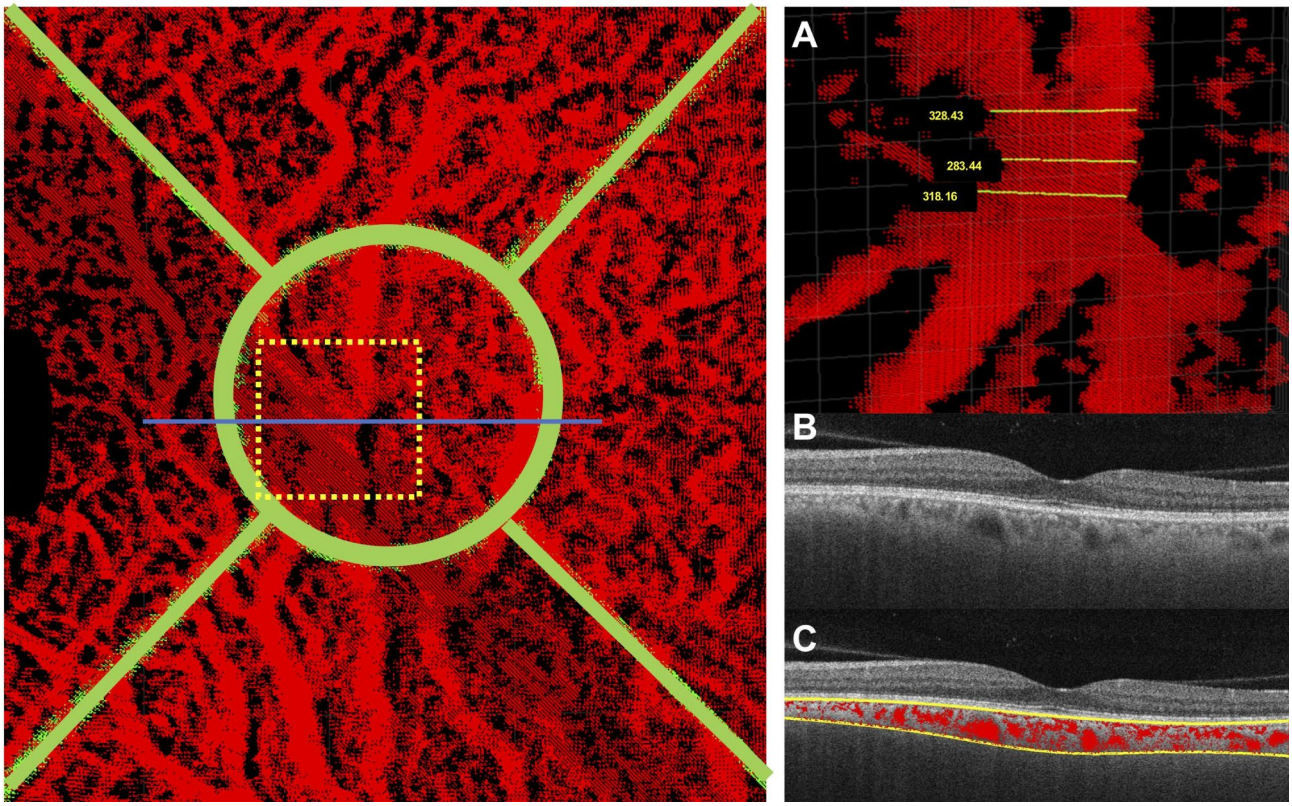

Fig. 4. Choroidal vessels in a healthy 53-year-old male. The image on the left shows the 3D en-face image. The magnified image (yellow square) and the OCT B-scan (blue line) are shown on the right. (A) In the central sector, the mean of the three measurements for the largest choroidal vessel was 310 µm. The vessel had a vertical pathway. (B) The correspondent OCT B-scan is shown. Note how the OCT B-scan is not effective in depicting the intricate anatomy of the vessel. (C) The corresponding binarization is shown.

size and show signs of cellular senescence, whereas choroidal melanocytes tend to fuse, forming rosette-like structures consisting of 8–15 cells. Overall, our results support the hypothesis that CVI decreases with age, and that vascular changes may occur predominantly in the choriocapillaris and the Sattler layer, with a preserved choroidal vessel diameters and relationship between vessels in the Haller layer over the years.

To the best of our knowledge, this is the first study observing a higher CVI in females compared to males. In a previous study, Mori et al. reported a higher CVI in men than women[23]. Also, Sonoda et al. showed an increased ratio of luminal to stromal area in males compared to females[24]. Since these studies were conducted using single OCT B-scans centered on the fovea, our findings suggest that differences in MChVD, CVI and IVD between genders may involve the extra-foveal region, with females exhibiting a higher CVI, MChVD and IVD compared to males. The clinical relevance of these metrics lies in their potential to uncover variations in vessel caliber and mean distance between vessels in 3D, which may significantly differ in healthy and pathological eyes. Such differences may have implications for understanding disease mechanisms. Therefore, further studies are needed to determine whether these findings are consistent across larger cohorts, in order to clarify the physiological and pathophysiological significance of these observations.

We observed that the sector with the highest MChVD was the inferior, followed by the superior, nasal, temporal and central. CT was thickest in the central sector, but it did not correlate with the MChVD. On the other hand, we observed a positive correlation between CT and MChVD in the temporal and superior sectors. Overall, our results support the hypothesis that the Haller layer influences choroidal thickness in certain regions, but the Sattler layer and choriocapillaris also might play a role in modulating choroidal thickness in different sectors, including the central sector. Several studies assessed the CT in both the macula and the peripheral retina, reporting different results secondary to variations in methodological techniques and the OCTs employed[25–27]. In a previous study, Hirano et al. reported that the posterior pole choroidal thicknesses in OCT B-scans of healthy eyes were significantly lower at the periphery than in the central area, in the inferior field than in the superior field, and in the nasal field than in the temporal field. They also suggested that the course of the short posterior ciliary arteries, the location of the watershed zones, the effect of gravity and the pathway of choroidal veins may influence the CT in different sectors[25]. To the best of our knowledge, this is the first study to measure the 3D choroidal vessels diameter in healthy eyes. We believe that further studies are needed to understand the effect of the watershed zones and the choroidal venous drainage in modulating the CT, MChVD and IVD in different sectors of choroid in healthy eyes.

	18–34 years old (patients = 20, eyes = 28)	35–59 years old (patients = 19, eyes = 30)	> 60 years old (patients 13, eyes = 22)	*P* value
Choroidal thickness (μm), mean ± SD				
Mean	303.6 ± 64.0	294.0 ± 61.6	239.1 ± 58.8	**0.009**
Nasal	247.2 ± 60.5	258.0 ± 66.4	223.2 ± 60.3	0.127
Temporal	305.2 ± 60.6	298.3 ± 78.5	229.7 ± 52.8	**0.003**
Inferior	322.3 ± 62.3	300.8 ± 77.6	266.6 ± 72.5	0.096
Superior	312.1 ± 75.9	306.1 ± 67.8	230.3 ± 61.5	**0.002**
Central	331.3 ± 81.5	326.9 ± 82.0	257.9 ± 69.5	**0.017**
Choroidal vascularity index (μm), mean ± SD				
Mean	42.0 ± 2.0	39.9 ± 2.8	38.7 ± 2.5	**0.002**
Nasal	41.9 ± 4.2	39.9 ± 3.0	37.5 ± 3.8	**0.004**
Temporal	41.2 ± 2.0	39.5 ± 2.0	37.2 ± 3.4	**< 0.001**
Inferior	42.2 ± 2.2	40.9 ± 2.2	39.7 ± 2.1	**0.005**
Superior	43.6 ± 2.2	42.0 ± 1.8	40.4 ± 3.3	**0.001**
Central	41.3 ± 2.6	40.0 ± 1.9	38.8 ± 3.2	**0.014**
Mean choroidal vessel diameter (MChVD) (μm), mean ± SD				
Mean	201.6 ± 23.3	205.7 ± 20.0	191.5 ± 32.6	0.330
Nasal	200.3 ± 33.0	202.6 ± 35.8	194.0 ± 64.7	0.843
Temporal	201.7 ± 33.9	198.8 ± 39.0	181.6 ± 45.2	0.283
Inferior	207.5 ± 30.2	216.3 ± 37.0	212.8 ± 50.5	0.687
Superior	207.7 ± 31.0	209.0 ± 41.4	199.1 ± 41.1	0.869
Central	190.6 ± 45.0	202.5 ± 32.3	185.8 ± 43.4	0.405
Inter-vessel distance (IVD) (μm), mean ± SD				
Mean	178.3 ± 31.4	200.4 ± 33.7	174.1 ± 35.8	0.054
Nasal	171.5 ± 40.5	189.1 ± 45.0	168.7 ± 55.3	0.263
Temporal	181.7 ± 50.9	205.3 ± 55.1	174.0 ± 50.3	0.100
Inferior	174.4 ± 43.1	208.0 ± 48.6	172.8 ± 43.3	**0.035**
Superior	178.0 ± 45.3	198.0 ± 49.8	191.2 ± 52.2	0.443
Central	186.0 ± 39.6	200.9 ± 46.9	164.0 ± 45.5	**0.039**

Table 3. Three-dimensional choroidal vascular biomarkers in different age groups. *SD* standard deviation; *MChVD* mean choroidal vessel diameter; *IVD* inter-vessel distance. Significant values are in bold.

In the present study, we observed a significant decrease in mean CT with age. On the other hand, we did not observe a significant reduction in mean CT with increasing AL. Wakatsuki et al. reported a decrease in the subfoveal choroidal thickness by 2.98 μm each year of advancing age[28]. Also, Flores-Moreno et al. reported that choroidal thickness decreased by 25.9 ± 2.1 μm for each additional millimeter in the axial length[29]. Recently, Hirano et al. reported that CT was negatively associated with advanced age using two-dimensional wide-field SS-OCT, suggesting that choroidal thinning with age occurs both in the macula and in the peripheral retina. Furthermore, they observed that choroidal thickness was negatively associated with axial length in the central and inferonasal sectors[25]. Although the results generally show a reduction in CT with increasing age and axial length, the discrepancies between studies may arise from variations in methodological techniques and the machines employed. In the present study, we excluded eyes with an AL inferior to 22 mm and superior to 26 mm. Therefore, future studies including eyes with different axial lengths are needed to explore changes in choroidal biomarkers in 3D maps.

One of the biggest challenges with choroidal vessel assessment has been two-dimensional evaluation of these intersecting vessels in different planes, thus the diameter evaluation has never been reliable. The diameter of choroidal vessel is increasing more valuable due to its relationship with pathogenic mechanisms in various diseases such as pachychoroid disease spectrum. As the previous studies have reported choroidal vessel diameter in B scan or en-face images which cannot be used reliably, our study reports authentic values for diameter, and can establish the database for future studies. Furthermore, MChVD and IVD may represent two novel biomarkers for the assessment of the choroidal structure. Previously, Yang et al. reported that the mean diameter of the largest choroidal vessel under the fovea was 140 μm in healthy controls, compared to 305 in the eyes with central serous chorioretinopathy assessed using OCT B-scans[30]. In the present study, we observed that 33% of the eyes presented at least one choroidal vessel larger than 200 μm crossing the central 3000 μm of the macula. To the best of our knowledge, this is the first study reporting an objective method to quantify single choroidal vessels in 3D maps and define their morphological features. This method is effective in understanding the intricate anatomy of the choroidal vessels, their collateral vessels and their spatial relationship with adjacent vessels. Overall, these results suggest that one-third of healthy eyes present at least one large choroidal vessel in the central macula, even in the absence of pathological conditions. We chose 200 microns as a new cut-off for large choroidal vessels crossing the fovea. This decision was not pre-determined based on existing physiological

	Male (patients = 24, eyes = 36)	Female (patients = 29, eyes = 44)	*P* value
Choroidal thickness (μm), mean ± SD			
Mean	294.9 ± 81.4	272.0 ± 50.2	0.364
Nasal	252.1 ± 73.3	238.6 ± 54.4	0.504
Temporal	291.1 ± 88.6	274.2 ± 56.8	0.697
Inferior	308.7 ± 84.7	291.6 ± 62.9	0.636
Superior	305.5 ± 92.3	271.8 ± 58.2	0.141
Central	325.5 ± 95.3	296.4 ± 71.9	0.347
Choroidal vascularity index (μm), mean ± SD			
Mean	39.7 ± 2. 9	40. 9 ± 2.6	0.079
Nasal	39.1 ± 4.5	40.6 ± 3.5	0.110
Temporal	38.7 ± 3.4	40.1 ± 2.3	**0.031**
Inferior	40.6 ± 2.2	41.4 ± 2.4	0.110
Superior	41.6 ± 2.6	42.6 ± 2.7	0.078
Central	39.7 ± 2.9	40.5 ± 2.5	0.181
Mean choroidal vessel diameter (MCVD) (μm), mean ± SD			
Mean	195.2 ± 25. 9	204.6 ± 24.4	0.161
Nasal	185.4 ± 43.0	210.9 ± 42.6	**0.019**
Temporal	191.3 ± 43.1	198.2 ± 36.6	0.514
Inferior	207.9 ± 37.6	215.7 ± 39.4	0.380
Superior	204.5 ± 40.0	206.9 ± 36.2	0.622
Central	188.7 ± 42.1	197.9 ± 38.8	0.376
Inter-vessel distance (IVD) (μm), mean ± SD			
Mean	175.9 ± 28.7	193.1 ± 38.1	0.165
Nasal	169.3 ± 42.2	183.9 ± 49.9	0.271
Temporal	182.6 ± 46.3	193.3 ± 58.7	0.464
Inferior	181.9 ± 47.5	190.2 ± 48.1	0.846
Superior	174.3 ± 47.2	201.3 ± 47.8	**0.034**
Central	173.5 ± 195.4	195.4 ± 49.7	0.066

Table 4. Three-dimensional choroidal vascular biomarkers according to the sex of the patients. *SD* standard deviation; *MChVD* mean choroidal vessel diameter; *IVD* inter-vessel distance. Significant values are in bold.

data, but rather was made to provide a useful starting point for future 3D vessel studies. Furthermore, we found that the pathways of the large choroidal vessels were predominantly oblique in 62% of the cases, vertical in 29%, and horizontal in 7%. We believe that understanding these pathways in 3D maps could provide valuable insights into choroidal outflow dynamics and enhance our understanding of choroidal circulation, as well as its role in retinal pathologies in future research.

The current study has certain limitations. The sample size used in our study was relatively small. Including a larger sample size would have added greater robustness to the findings. Also, we included in the study an area of 6 × 6 mm area, due to which, the peripheral choroid, including the assessment of the vortex veins, was not investigated. Therefore, some of the largest vessels evaluated in this study may represent a confluence of collecting veins rather than a single large vessel. Our future goal is to employ ultra-widefield imaging to assess the peripheral retina, enabling a clearer distinction between vascular branches and trunks. Furthermore, as this was a retrospective cross-sectional study, we could not evaluate the long-term changes in healthy eyes at different ages, to understand if Haller choroidal vessels present changes with increasing age. Therefore, further prospective studies with an increased cohort of patients are needed to better understand our findings. Another limitation of the current study was that the selection and measurement of the three largest choroidal vessels and the IVD per sector required an assessment by trained observers. To obtain objective measurements, the images were rotated to provide a comprehensive three-dimensional view, and only the three largest vessels per sector were included in the analysis. Furthermore, we observed a good reliability between the two graders, suggesting consistency in the measurements. However, further research is needed to fully automate the selection of the largest vessels, the inter-vessel distance per sector, and their measurements.

Conclusions

In the present study, we observed that CT and CVI decreased with increasing age. However, MChVD and IVD did not present any changes in different age groups, suggesting that vascular changes with aging in healthy eyes occur predominantly in the choriocapillaris and the Sattler layers, with a preserved Haller layer over the years. Also, CVI, MChVD and IVD were increased in healthy females compared to males, suggesting that differences in CVI and choroidal diameter and spacing between sexes may involve the extra-foveal region. Furthermore, we observed that one-third of patients presented at least one choroidal vessel larger than 200 μm crossing the

Univariable model	Coefficient (95% CI)	*P* value
Choroidal thickness		
Mean	− 1.31 (− 2.06 to − 0.55)	**0.001**
Nasal	− 0.57 (− 1.33 to 0.18)	0.135
Temporal	− 1.41 (− 2.28 to − 0.65)	**0.001**
Inferior	− 1.17 (− 2.02 to − 0.31)	**0.008**
Superior	− 1.67 (− 2.52 to − 0.82)	< **0.001**
Central	− 1.54 (− 2.49 to − 0.54)	**0.002**
Choroidal vascularity index (CVI)		
Mean	− 0.07 (− 0.10 to − 0.04)	< **0.001**
Nasal	− 0.11 (− 0.15 to − 0.06)	< **0.001**
Temporal	− 0.09 (− 0.12 to − 0.06)	< **0.001**
Inferior	− 0.05 (− 0.11 to 0.01)	0.071
Superior	− 0.07 (− 0.13 to − 0.01)	**0.025**
Central	− 0.05 (− 0.08 to − 0.02)	**0.001**
Mean choroidal vessel diameter (MCVD)		
Mean	− 0.10 (− 0.41 to 0.19)	0.482
Nasal	0.12 (− 0.66 to 0.40)	0.637
Temporal	− 0.41 (− 0.88 to 0.05)	0.085
Inferior	0.22 (− 0.24 to 0.68)	0.349
Superior	− 0.02 (− 0.48 to 0.43)	0.921
Central	− 0.42 (− 0.53 to 0.44)	0.865
Inter-vessel distance (IVD)		
Mean	0.05 (− 0.429 to 0.38)	0.801
Nasal	− 0.12 (− 0.68 to 0.44)	0.672
Temporal	0.002 (− 0.64 to 0.65)	0.995
Inferior	0.07 (− 0.51 to 0.65)	0.811
Superior	0.34 (− 0.24 to 0.93)	0.243
Central	− 0.31 (− 0.87 to 0.23)	0.255

Table 5. Association of 3D choroidal biomarkers with age. Significant values are in bold.

central 3000 µm of the macula. To the best of our knowledge, this is the first study reporting an objective method to quantify single choroidal vessels in 3D maps and define their characteristics. The 3D evaluation of choroidal vessels using a deep-learning approach is an innovative and non-invasive technique that allows for detailed analysis of the morphology and diameters of choroidal vessels. This technology holds promise for advancing our understanding of the pathophysiological mechanisms underlying chorioretinal disorders, with the potential of being applied in clinical practice in the future.

Univariable model	Coefficient (95% CI)	*P* value
Choroidal thickness		
Mean	− 3.52 (− 23.1 to 8.7)	0.278
Nasal	− 8.2 (− 29.0 to 12.4)	0.426
Temporal	− 3.2 (− 22.7 to 16.1)	0.734
Inferior	− 2.17 (− 4.12 to − 0.11)	**0.008**
Superior	− 3.61 (− 5.56 to − 1.52)	**0.006**
Central	− 2.14 (− 4.39 to − 0.84)	**0.003**
Choroidal vascularity index (CVI)		
Mean	0.04 (− 0.82 to 0.91)	0.622
Nasal	− 1.22 (− 2.49 to 0.05)	0.061
Temporal	− 0.08 (− 0.86 to 0.69)	0.827
Inferior	− 0.19 (− 0.95 to 0.57)	0.610
Superior	1.63 (− 0.49 to 3.77)	0.130
Central	0.10 (− 0.80 to 1.01)	0.822
Mean choroidal vessel diameter (MCVD)		
Mean	− 7.59 (− 15.89 to 0.70)	0.072
Nasal	− 15.8 (− 30.4 to − 1.23)	**0.034**
Temporal	− 5.9 (− 0.88 to 0.05)	0.085
Inferior	0.22 (− 0.24 to 0.68)	0.349
Superior	− 0.02 (− 0.48 to 0.43)	0.921
Central	− 0.42 (− 0.53 to 0.44)	0.865
Inter-vessel distance (IVD)		
Mean	− 6.77 (− 15.85 to 2.30)	0.139
Nasal	− 2.1 (− 15.9 to 4.0)	0.219
Temporal	− 15.7 (− 29.9 to − 1.5)	**0.030**
Inferior	− 12.4 (− 25.0 to 0.1)	0.051
Superior	− 2.1 (− 15.2 to 10.8)	0.736
Central	− 0.7 (− 13.1 to 11.5)	0.902

Table 6. Association of 3D choroidal biomarkers with axial length. Significant values are in bold.

Data availability

The datasets used and analyzed during the current study are available from the corresponding author upon reasonable request.

Received: 25 August 2024; Accepted: 1 January 2025
Published online: 03 January 2025

References

1. Brinks, J. et al. Exploring the choroidal vascular labyrinth and its molecular and structural roles in health and disease. *Prog Retin Eye Res.* **87**, 100994. https://doi.org/10.1016/j.preteyeres.2021.100994 (2022).
2. Nickla, D. L. & Wallman, J. THE MULTIFUNCTIONAL CHOROID. *Prog Retin Eye Res.* **29** (2), 144–168. https://doi.org/10.1016/j.preteyeres.2009.12.002 (2010).
3. Branchini, L. A. et al. Analysis of choroidal morphologic features and vasculature in healthy eyes using spectral-domain optical coherence tomography. *Ophthalmology* **120** (9), 1901–1908. https://doi.org/10.1016/j.ophtha.2013.01.066 (2013).
4. Singh, S. R., Vupparaboina, K. K., Goud, A., Dansingani, K. K. & Chhablani, J. Choroidal imaging biomarkers. *Surv. Ophthalmol.* **64** (3), 312–333. https://doi.org/10.1016/j.survophthal.2018.11.002 (2019).
5. Iovino, C. et al. Choroidal Vascularity Index: an In-Depth analysis of this Novel Optical Coherence Tomography parameter. *J. Clin. Med.* **9** (2), 595. https://doi.org/10.3390/jcm9020595 (2020).
6. Agrawal, R. et al. Choroidal vascularity index as a measure of vascular status of the choroid: measurements in healthy eyes from a population-based study. *Sci. Rep.* **6**, 21090. https://doi.org/10.1038/srep21090 (2016).
7. Singh, S. R. et al. En-face choroidal vascularity map of the macula in healthy eyes. *Eur. J. Ophthalmol.* **31** (1), 218–225. https://doi.org/10.1177/1120672119883593 (2021).
8. Ung, C. et al. Evaluation of choroidal lesions with swept-source optical coherence tomography. *Br. J. Ophthalmol.* **103** (1), 88–93. https://doi.org/10.1136/bjophthalmol-2017-311586 (2019).
9. Drexler, W. et al. Optical coherence tomography today: speed, contrast, and multimodality. *J. Biomed. Opt.* **19** (7), 071412. https://doi.org/10.1117/1.JBO.19.7.071412 (2014).
10. Vupparaboina, K. K. et al. Automated choroid layer segmentation based on wide-field SS-OCT images using deep residual encoder-decoder architecture. *Investig. Ophthalmol. Vis. Sci.* **62** (8), 2162 (2021).
11. Kugelman, J. et al. Automatic choroidal segmentation in OCT images using supervised deep learning methods. *Sci. Rep.* **9** (1), 13298. https://doi.org/10.1038/s41598-019-49816-4 (2019).
12. Masood, S. et al. Automatic choroid layer segmentation from Optical Coherence Tomography images using deep learning. *Sci. Rep.* **9** (1), 3058. https://doi.org/10.1038/s41598-019-39795-x (2019).

13. Chen, H. J. et al. Application of Artificial Intelligence and Deep Learning for Choroid Segmentation in Myopia. *Transl Vis. Sci. Technol.* **11** (2), 38. https://doi.org/10.1167/tvst.11.2.38 (2022).
14. Ibrahim, M. N. et al. Volumetric quantification of choroid and Haller's sublayer using OCT scans: an accurate and unified approach based on stratified smoothing. *Comput. Med. Imaging Graph.* **99**, 102086. https://doi.org/10.1016/j.compmedimag.2022.102086 (2022).
15. Dansingani, K. K. et al. *Retina* ;**36**(3):499–516. https://doi.org/10.1097/IAE.0000000000000742 (2016).
16. Agrawal, R. et al. CHOROIDAL VASCULARITY INDEX IN CENTRAL SEROUS CHORIORETINOPATHY. *Retina* **36** (9), 1646–1651. https://doi.org/10.1097/IAE.0000000000001040 (2016).
17. Zeng, Q. et al. Three-dimensional choroidal vascularity index in central serous chorioretinopathy using ultra-widefield swept-source optical coherence tomography angiography. *Front. Med. (Lausanne)*. **9**, 967369. https://doi.org/10.3389/fmed.2022.967369 (2022).
18. Accurate Detection of 3D Choroidal Vasculature Using Swept-Source OCT Volumetric Scans Based on Phansalkar Thresholding. html. Accessed April 19. (2024). https://bhiconference.github.io/BHI2023/2023/1570919296.html
19. Sadeghi, E. et al. Three-Dimensional Choroidal vessels Assessment in Age-Related Macular Degeneration. *Invest. Ophthalmol. Vis. Sci.* **65** (13), 39. https://doi.org/10.1167/iovs.65.13.39 (2024).
20. Yang, J., Wang, E., Yuan, M. & Chen, Y. Three-dimensional choroidal vascularity index in acute central serous chorioretinopathy using swept-source optical coherence tomography. *Graefes Arch. Clin. Exp. Ophthalmol.* **258** (2), 241–247. https://doi.org/10.1007/s00417-019-04524-7 (2020).
21. Ruiz-Medrano, J. et al. *Retina* ;**38**(3):508–515. https://doi.org/10.1097/IAE.0000000000001571 (2018).
22. Xuan, M. et al. Distribution and determinants of choroidal vascularity index in healthy eyes from deep-learning choroidal analysis: a population-based SS-OCT study. *Br. J. Ophthalmol.* **108** (4), 546–551. https://doi.org/10.1136/bjo-2023-323224 (2024).
23. Mori, Y. et al. Distribution of Choroidal Thickness and Choroidal Vessel Dilation in healthy Japanese individuals. *Ophthalmol. Sci.* **1** (2), 100033. https://doi.org/10.1016/j.xops.2021.100033 (2021).
24. Sonoda, S. et al. Luminal and stromal areas of choroid determined by binarization method of optical coherence tomographic images. *Am. J. Ophthalmol.* **159** (6), 1123–1131e1. https://doi.org/10.1016/j.ajo.2015.03.005 (2015).
25. Hirano, M. et al. Analysis of widefield choroidal thickness maps of healthy eyes using swept source optical coherence tomography. *Sci. Rep.* **13** (1), 11904. https://doi.org/10.1038/s41598-023-38845-9 (2023).
26. Xie, R., Qiu, B., Chhablani, J. & Zhang, X. Evaluation of Choroidal Thickness using Optical Coherent Tomography: a review. *Front. Med. (Lausanne)*. **8**, 783519. https://doi.org/10.3389/fmed.2021.783519 (2021).
27. Touhami, S. et al. Topographic variations of Choroidal Thickness in healthy eyes on swept-source Optical Coherence Tomography. *Investig. Ophthalmol. Vis. Sci.* **61** (3), 38. https://doi.org/10.1167/iovs.61.3.38 (2020).
28. Wakatsuki, Y., Shinojima, A., Kawamura, A. & Yuzawa, M. Correlation of Aging and Segmental Choroidal Thickness Measurement using swept source optical coherence tomography in healthy eyes. *PLoS One.* **10** (12), e0144156. https://doi.org/10.1371/journal.pone.0144156 (2015).
29. Flores-Moreno, I., Lugo, F., Duker, J. S. & Ruiz-Moreno, J. M. The relationship between axial length and Choroidal thickness in eyes with high myopia. *Am. J. Ophthalmol.* **155** (2), 314–319e1. https://doi.org/10.1016/j.ajo.2012.07.015 (2013).
30. Yang, L., Jonas, J. B. & Wei, W. Choroidal vessel diameter in central serous chorioretinopathy. *Acta Ophthalmol.* **91** (5), e358–362. https://doi.org/10.1111/aos.12059 (2013).

Author contributions

N.V. collecting data, analyzing images, and writing. E.S. collecting data, analyzing images, and writing. E.D. analyzing images. M.N.I. conceptualizing, methodology, software development. N.H. writing. S.C.B. conceptualizing, methodology, software development. S.R.S. conceptualizing. L.F. supervision. J.A.S supervision. K.K.V. conceptualizing, supervision, methodology, software development. J.C. conceptualizing, supervision, methodology, and writing. All authors read and approved the final version.

Funding

This work was supported by NIH CORE Grant P30 EY08098 to the Department of Ophthalmology, the Eye and Ear Foundation of Pittsburgh, and from an unrestricted grant from Research to Prevent Blindness, New York, NY.

Declarations

Competing interests

The authors declare no competing interests.

Ethics approval and consent to participate

All participants gave written informed consent. The study was approved by the local ethics committee. The patients did not receive any financial compensation for their participation. The patients were advised that the data collected were used for scientific purposes and they gave their consent for publication.

Additional information

Supplementary Information The online version contains supplementary material available at https://doi.org/10.1038/s41598-025-85189-7.

Correspondence and requests for materials should be addressed to J.C.